

Formation Routes of CO from O(^{1}D)+Toluene: A Computational Study

Marzio Rosi[1(✉)], Piergiorgio Casavecchia[2], Nadia Balucani[2], Pedro Recio[2], Adriana Caracciolo[3], Dimitrios Skouteris[4], and Carlo Cavallotti[5]

[1] Department of Civil and Environmental Engineering, University of Perugia, 06125 Perugia, Italy
marzio.rosi@unipg.it
[2] Department of Chemistry, Biology and Biotechnologies, University of di Perugia, 06123 Perugia, Italy
{piergiorgio.casavecchia,nadia.balucani}@unipg.it
[3] Ann and H.J. Smead, Department of Aerospace Engineering Sciences, University of Colorado, Boulder, CO 80303, USA
adriana.caracciolo@colorado.edu
[4] Master-Tec, 06128 Perugia, Italy
[5] Department of Chemistry, Materials and Chemical Engineering, Politecnico di Milano, 20131 Milan, Italy
carlo.cavallotti@polimi.it

Abstract. The interaction between oxygen atoms in their first electronically excited state ^{1}D with toluene has been characterized by electronic structure calculations. We focused our attention, in particular, on the different pathways leading to the formation of CO. Six different reaction channels have been investigated. Our results suggest that, while for accurate energies high level calculations, as CCSD(T), are necessary, in particular when strong correlation effects are present, for semi-quantitative results DFT methods are adequate and provide information useful when larger systems than toluene as polycyclic aromatic hydrocarbons are under investigation.

Keywords: Computational chemistry · Ab initio calculations · Density functional theory methods · Coupled clusted calculations · Combustion · Fuels

1 Introduction

The bimolecular reaction between atomic oxygen in its ground state ^{3}P and first excited state ^{1}D and toluene is extremely important in combustion chemistry since toluene is the major aromatic found in gasoline. To understand the kinetics of toluene oxidation is necessary to know the primary products and the branching ratios of the bimolecular reactions O(^{3}P, ^{1}D)+toluene as a function of temperature and pressure. Despite extensive kinetic studies [1–4], little is known about the mechanism and branching fractions of this reaction. We have therefore undertaken a synergistic experimental and theoretical

© The Author(s), under exclusive license to Springer Nature Switzerland AG 2022
O. Gervasi et al. (Eds.): ICCSA 2022 Workshops, LNCS 13378, pp. 260–269, 2022.
https://doi.org/10.1007/978-3-031-10562-3_19

investigation of the reactions O(3P, 1D)+toluene with the same approach recently used to identify all primary products and determine the branching fractions for the reactions of O (3P, 1D) with a variety of unsaturated aliphatic and aromatic hydrocarbons [5–10]. This approach consists in experiments performed using the crossed molecular beam technique with soft electron ionization mass spectrometric detection and time-of-flight analysis. The experimental results are combined with electronic structure calculations of the triplet and singlet potential energy surfaces and statistical RRKM/Master Equation kinetic computations. In this way, the product distribution as a function of collision energy, as well as temperature and pressure, with intersystem crossing taken into account, is obtained and provides important information for improved kinetic modeling of toluene combustion.

We have recently investigated both experimentally and theoretically [9, 10] the reaction between O in the ground 3P state and the first excited 1D state and benzene. The main products are atomic hydrogen and carbon monoxide; hydrogen can be formed both in the triplet and in the singlet surfaces while CO can be formed only in the singlet surface starting form O(1D) or via intersystem crossing. Preliminary experimental information on the reaction O(1D, 3P)+toluene suggest that the main products are H, CH_3 and CO. For analogy with the reaction O(1D, 3P)+benzene we expect that H and CH_3 could be formed both in the singlet and triplet surfaces, while CO should be formed only in the singlet surface.

In this contribution we present the study of the singlet surface O(1D)+toluene focusing our attention to the formation of CO. The interaction with the triplet O(3P) surface via intersystem crossing will be the subject of future investigations.

2 Theoretical Methods

The evaluation of the potential energy surface of O(1D)+toluene has been performed at Density Functional Theory (DFT) level of calculation optimizing the stationary points (minima and transition states) using the ωB97X-D [11, 12] functional, and the 6–311+G(d,p) basis set [13, 14]. The same level of theory has been used to evaluate the vibrational frequencies in order to establish the nature of the stationary point, i.e. minimum if all the frequencies are real, transition state if there is one, and only one, imaginary frequency. Moreover, In order to assign the saddle points to the relative reactants and products we performed intrinsic reaction coordinate (IRC) calculations [15, 16] The energy of all the stationary points was computed at a more accurate level of approximation performing CCSD(T) calculations [17–19] using the correlation consistent aug-cc-pVTZ basis set [20] and the DFT optimized geometries. This computational scheme has been previously successfully applied [21–35]. Both the DFT and the CCSD(T) energies were corrected to 0 K by adding the zero point energy correction computed using the scaled harmonic vibrational frequencies evaluated at DFT level. The energy of O(1D) was estimated by adding the experimental [36] separation O(3P) – O(1D) of 45.3 kcal mol^{-1} to the energy of O(3P) at all levels of calculation. All calculations were done using Gaussian 09 [37] while the analysis of the vibrational frequencies was performed using Molekel [38, 39].

3 Results and Discussion

3.1 O(^{1}D)+Toluene

Figure 1 reports the optimized geometries at ωB97X-D/6–311+G(d,p) level of the isomers deriving from the interaction of oxygen in its excited ^{1}D state with toluene. We have three different isomers depending on the carbon atoms interacting with oxygen, which are almost degenerate: species **2** is only 1.4 kcal/mol less stable than isomer **1**, while species **3** is 1.8 kcal/mol above species **1** at ωB97X-D/6–311+G(d,p) level of calculation. At CCSD(T)/aug-cc-pVTZ//ωB97X-D/6–311+G(d,p) level of theory, the relative energies are almost the same: species **2** is 1.8 kcal/mol less stable than **1** while **3** is 1.9 kcal/mol less stable than **1**. O(^{1}D) is able to form two σ bonds with two adjacent carbon atoms, because it has two electrons with opposite spin in different *p* orbitals. These electrons interact with the two electrons with opposite spin involved in the π bond of the two carbon atoms. The energy required for breaking the π bond is more than compensated by the energy associated to the formation of the two σ bonds between oxygen and carbon, as it is shown in Table 1 where the energetics of the reactions under investigation is reported. We can notice that the formation of species **1**, **2**, or **3** is exothermic by about 100 kcal/mol both at DFT and CCSD(T) level of calculation. In particular, the formation of **1** is exothermic by 100.4 kcal/mol at DFT level (100.7 at CCSD(T) level); the formation of **2** by 99.0 kcal/mol at DFT level (98.9 at CCSD(T) level) and that of **3** by 98.6 kcal/mol at DFT level (98.8 at CCSD(T) level). The breaking of the π bond is shown by the C—C bond distance reported in Fig. 1 which corresponds to that of a single bond for the carbon atoms interacting with oxygen, being 1.51 Å in **1** and 1.50 Å in **2** and **3**. From Fig. 1 we can notice that the oxygen atom bonds symmetrically to two adjacent carbon atoms, being the bond distances (1.43 Å in **1** and 1.42 Å in **2** and **3**) equal for both C—O bonds and correspond to a single σ bond. The first step towards the formation of CO is always an hydrogen shift between two adjacent carbon atoms. Starting from species **1** or species **2** the shift of an hydrogen from C2 to C1 leads to species **4** reported in Fig. 2. In species **4** the oxygen shows a double bond with C2 being the C—O distance only 1.22 Å. From species **2** we can have also the shift of an hydrogen from C3 to C4 with the formation of species **16**, while species **3** can show the shift of an hydrogen from C3 to C2 or from C4 to C5 giving rise to species **15** or **17**, respectively. Also in species **15**, **16** and **17** the oxygen atom shows a double bond with C3, C3 and C4, respectively.

In Fig. 3 we have reported the potential energy surface (PES) relative to the reactions leading to the formation of CO starting from the species reported in Fig. 1. We have two different panels, panel **a** reports the pathways originating from species **1** (and in part species **2**), while panel **b** reports the reactions starting from species **2** and **3**. The energy changes and barrier heights relative to these reactions are shown in Table 1 both at ωB97X-D/6–311+G(d,p) level of calculations and at the more accurate CCSD(T)/aug-cc-pVTZ//ωB97X-D/6–311+G(d,p) level of theory. In Fig. 3 for clarity only the CCSD(T)/aug-cc-pVTZ//ωB97X-D/6–311+G(d,p) energy values are reported.

Table 1. ΔH_0^0 and barrier heights (kcal/mol, 0 K) computed at DFT (CCSD(T)) level for the pathways leading to CO formation starting from O(^{1}D)+toluene. All the energies include zero point energy correction. For the numbering of the isomers see Fig. 3.

	ΔH_0^0	Barrier height
O(^{1}D)+$C_6H_5CH_3$ → 1	−100.4 (−100.7)	
O(^{1}D)+$C_6H_5CH_3$ → 2	−99.0 (−98.9)	
O(^{1}D)+$C_6H_5CH_3$ → 3	−98.6 (−98.8)	
1 → 4	24.2 (−22.8)	46.0 (47.8)
2 → 4	−25.6 (−24.6)	38.3 (40.8)
4 → 6	25.3 (26.4)	35.1 (35.1)
6 → 9	6.8 (5.8)	55.7 (53.6)
9 → 13+CO	−17.8 (−23.4)	29.9 (27.1)
4 → 5	−4.0 (−3.4)	36.5 (37.4)
5 → 8	37.5 (36.0)	42.4 (46.9)
8 → 12	−1.1 (−2.4)	9.4 (6.3)
12 → 14+CO	−19.2 (−24.5)	37.7 (33.1)
4 → 7	33.9 (33.0)	37.1 (38.1)
7 → 10	−5.0 (−2.6)	5.5 (6.1)
10 → 11+CO	−19.2 (−24.5)	29.6 (26.6)
2 → 16	−30.1 (−28.2)	44.8 (45.4)
16 → 20	43.3 (40.7)	45.9 (45.3)
20 → 22	−8.2 (−7.6)	3.4 (4.2)
22 → 14+CO	−18.2 (−23.8)	30.2 (28.7)
3 → 15	−30.3 (−28.0)	44.5 (45.4)
15 → 19	46.0 (43.6)	46.1 (45.1)
19 → 9	−10.8 (−8.1)	2.7 (2.7)
9 → 13+CO	−17.8 (−23.4)	29.9 (27.1)
3 → 17	−28.9 (−26.9)	40.4 (42.9)
17 → 18	40.9 (39.1)	44.3 (44.3)
18 → 21	−10.2 (−7.3)	3.3 (4.0)
21 → 11+CO	−18.1 (−23.7)	31.9 (29.9)

It is worth noting from Table 1 that the DFT and CCSD(T) energies are in reasonable agreement, the difference being about 2 – 3 kcal/mol. Only the dissociation reactions which show, as expected, more relevant correlation effects present a slightly larger energy difference (about 5 kcal/mol). This point suggests that for the study of larger systems it should be possible to use DFT calculations in order to provide at least semi-quantitative results. This approach could be used therefore for the study of the interaction of oxygen atoms with larger polycyclic aromatic hydrocarbons (PAH's) where accurate CCSD(T) calculations are unfeasible due to the size of the systems.

From Fig. 3 and Table 1 we can see that we have six different pathways leading to the formation of CO. Let us consider in details these reactions. We will refer only to the more accurate CCSD(T) energies for simplicity. From Fig. 3, panel **a**, we see that species **1** and **2** isomerize to species **4** through the shift of an hydrogen atom from the C in ortho to the C in ipso, overcoming an energy barrier of 47.8 and 40.8 kcal/mol, respectively. Species **4** is more stable than **1** by 22.2 and **2** by 24.6 kcal/mol, respectively. Species **4** can follow three different pathways in order to evolve towards the CO formation, which are shown in Fig. 3 panel **a** with different colors. Let us start with the blue path, which implies the following reactions: **4** → **6** → **9** → **13**+CO. In this pathway we can notice the opening of the 6 membered ring (**6**) followed by the formation of a 5 membered ring (**9**). This last step implies a relatively high energy barrier (53.6 kcal/mol). In the red pathway we have the following reactions: **4** → **5** → **8** → **12** → **14**+CO. This pathway implies an additional isomerization with respect to the blue one and shows an energy barrier of 46.9 kcal/mol for the isomerization **5** → **8**. The green pathway implies the isomerizations: **4** → **7** → **10** → **11**+CO. This seems to be the preferred reaction path since it implies relatively low barrier heights. CO can be formed also starting from species **2** and **3**, as it is shown in panel **b** of Fig. 3. Let us consider these reactions. We have three different pathways, all of them starting with the shift of an hydrogen atom from one carbon to another adjacent carbon atom. The blue pathway implies the reactions: **2** → **16** → **20** → **22** → **14**+CO. The highest energy barrier in this reaction scheme is the first one which is equal to 45.4 kcal/mol. The other two reaction paths start from isomer **3**. In the red path we have the reactions: **3** → **15** → **19** → **9** → **13**+CO; this last reaction is in common with the blue path of panel **a.** Also in this case the highest energy barrier is the one relative to the first isomerization (45.4 kcal/mol). In the green pathway we have the reactions: **3** → **17** → **18** → **21** → **11**+CO. In this case the highest barrier height is the second one relative to the isomerization **17** → **18** (44.3 kcal/mol).

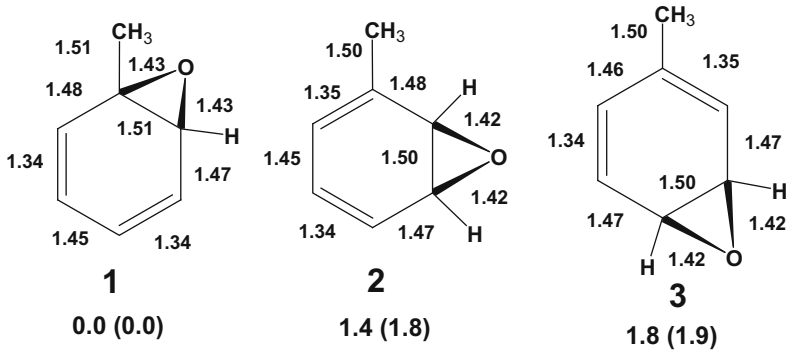

Fig. 1. Optimized geometries of the species obtained for the attack of O(^{1}D) to toluene. Geometry optimization has been performed at ωB97X-D/6–311+G(d,p) level. Bond lengths in Å. Relative energies (kcal/mol) with respect to species **1** have been evaluated at ωB97X-D/6–311+G(d,p) and, in parentheses, at CCSD(T)/aug-cc-pVTZ//ωB97X-D/6–311+G(d,p) level of theory.

In order to establish which is the preferred reaction pathway it is necessary to compute the branching fractions. For this purpose, RRKM calculations are under way. However, in the experimental conditions the presence of O(^{1}D) is only a minor part with respect to O(^{3}P). For this reason the main reaction path leading to the formation of CO should start form the triplet surface and through intersystem crossing should arrive to the singlet surface and to the final products as it is shown in our recent study of O+benzene [9, 10]. These calculations will be the subject of future work.

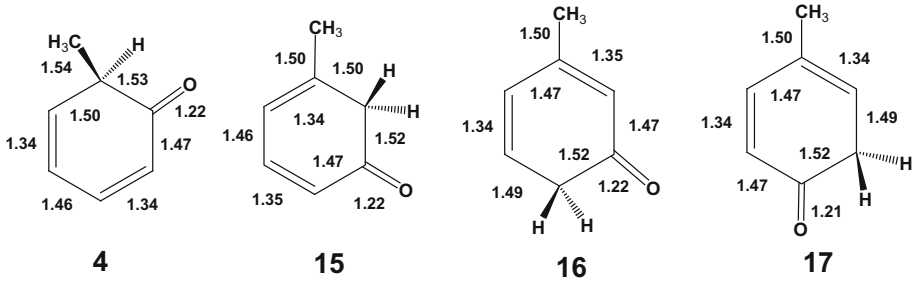

Fig. 2. Optimized geometries of the species involved in the first step of the reactive channels. Geometry optimization has been performed at ωB97X-D/6–311+G(d,p) level. Bond lengths in Å.

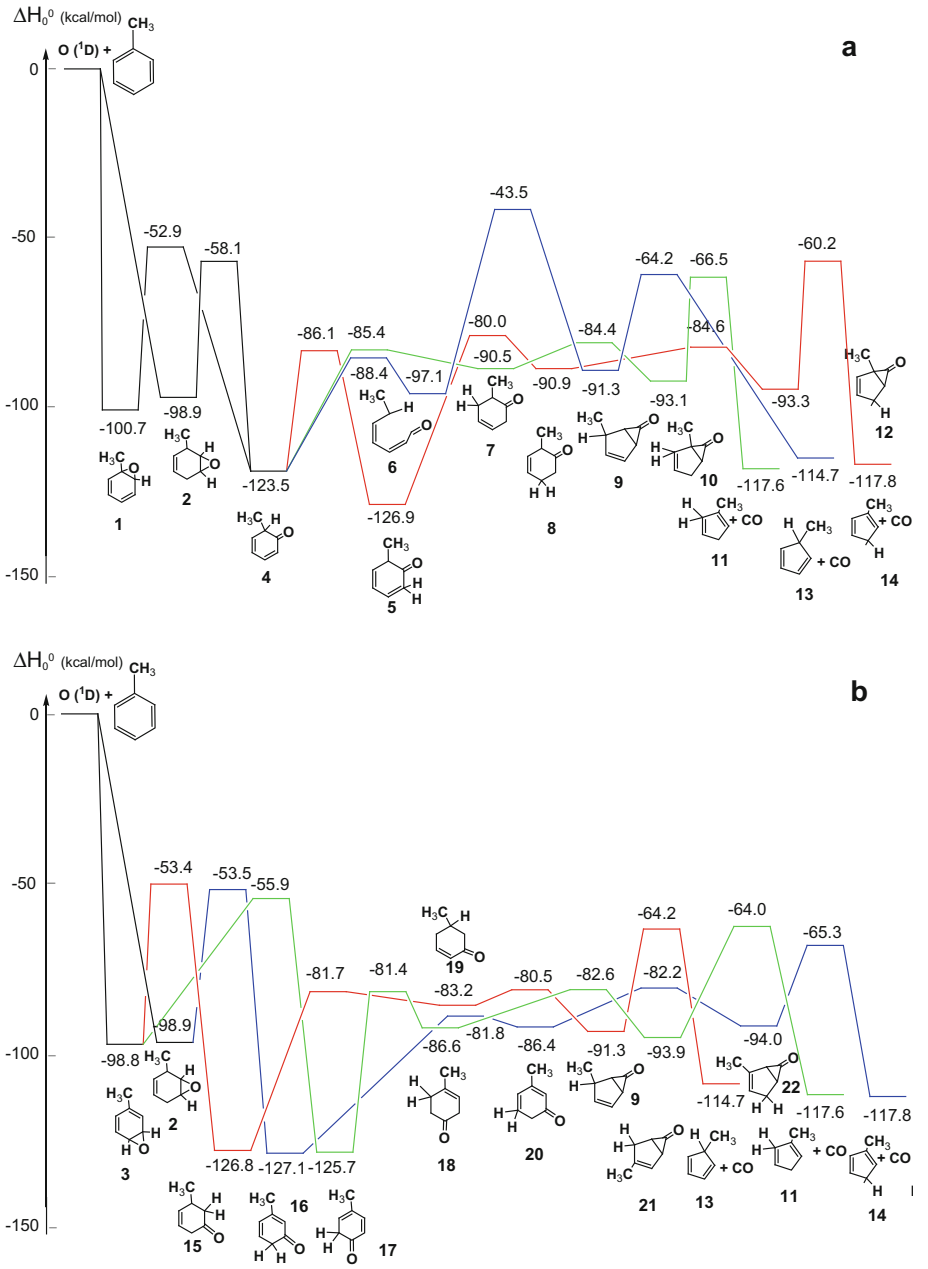

Fig. 3. Potential energy surface for the O(^{1}D)+toluene reaction. Only the pathways leading to the formation of CO are reported. Relative energies (kcal/mol) respect to O(^{1}D)+toluene, computed at CCSD(T)/aug-cc-pVTZ//ωB97X-D/6–311+G(d,p) level with inclusion of ZPE. In panel **a** pathways originating from isomer **1** are reported, while in panel **b** pathways originating from isomers **2** and **3** are shown.

4 Conclusions

The study at *ab initio* level of the interaction of O(^{1}D) with toluene, focusing the attention on the formation routes of CO, shows six possible different reaction channels. Although the potential energy surface provides information on the preferred exit channel through the barrier heights and the number of subsequent isomerization steps, the evaluation of branching fractions through RRKM calculations is necessary for a quantitative comparison. This will be the subject of future investigations The comparison between DFT and CCSD(T) calculations suggests that useful semi-quantitative results can be obtained also at DFT level of approximation. This is an important result in order to extend our study to complex PAHs.

Acknowledgments. The authors acknowledge the MUR (Italian Ministry of University and Research) for "PRIN 2017" funds, project MAGIC DUST, Grant Number 2017PJ5XXX. MR thanks the DICA, University of Perugia, for providing computing resources within the project "Dipartimenti di Eccellenza 2018–2022".

References

1. Brezinsky, K.: The high-temperature oxidation of aromatic hydrocarbons. Prog. Energy Combust. **12**, 1–24 (1986)
2. Atkinson, R., Pitts, J.N.: Rate constants for the reaction of O(^{3}P) atoms with Benzene and Toluene over the temperature range 299–440 K. Chem. Phys. Lett. **63**, 485–489 (1979)
3. Nicovich, J.M., Gump, C.A., Ravishankara, A.R.: Rates of reactions of O(^{3}P) with Benzene and Toluene. J. Phys. Chem. **86**, 1684–1690 (1982)
4. Tappe, M., Schliephake, V., Wagner, H.: Gg. reactions of Benzene, Toluene and Ethylbenzene with Atomic Oxygen O(^{3}P) in the Gas Phase Z. Phys. Chem. **162**, 129–145 (1989)
5. Cavallotti, C., et al.: Relevance of the channel leading to Formaldehyde + Triplet Ethylidene in the O(^{3}P)+Propene reaction under combustion conditions. J. Phys. Chem. Lett. **5**, 4213–4218 (2014)
6. Leonori, F., et al.: Experimental and theoretical studies on the dynamics of the O(^{3}P) + Propene reaction: primary products, branching ratios, and role of intersystem crossing. J. Phys. Chem. C **119**, 14632–14652 (2015)
7. Gimondi, I., Cavallotti, C., Vanuzzo, G., Balucani, N., Casavecchia, P.: Reaction dynamics of O(^{3}P)+Propyne: II. Primary products, branching ratios, and role of intersystem crossing from Ab initio coupled triplet/singlet potential energy surfaces and statistical calculations. J. Phys. Chem. A **120**, 4619–4633 (2016)
8. Caracciolo, A., et al.: Combined experimental and theoretical studies of the O(^{3}P) + 1-Butene reaction dynamics: primary products, branching ratios and role of intersystem crossing. J. Phys. Chem. A **123**, 9934–9956 (2019)
9. Cavallotti, C., et al.: A theoretical study of the extent of intersystem crossing in the O(^{3}P) + C_6H_6 reaction with experimental validation. J. Phys. Chem. Lett. **11**, 9621–9628 (2020)
10. Vanuzzo, G., et al.: Crossed-beam and theoretical studies of the O(^{3}P, ^{1}D) + Benzene reactions: primary products, branching fractions, and role of intersystem crossing. J. Phys. Chem. A **125**, 8434–8453 (2021)
11. Chai, J.-D., Head-Gordon, M.: Long-range corrected hybrid density functionals with damped atom-atom dispersion corrections. Phys. Chem. Chem. Phys. **10**, 6615–6620 (2008)

12. Chai, J.-D., Head-Gordon, M.: Systematic optimization of long-range corrected hybrid density functionals. J. Chem. Phys. **128**, 084106 (2008)
13. Krishnan, R., Binkley, J.S., Seeger, R., Pople, J.A.: Self-consistent molecular orbital methods. XX. A basis set for correlated wave functions. J. Chem. Phys. **72**, 650–654 (1980)
14. Frisch, M.J., Pople, J.A., Binkley, J.S.: Self-consistent molecular orbital methods 28. Supplementary functions for Gaussian basis sets. J. Chem. Phys. **80**, 3265–3269 (1984)
15. Gonzalez, C., Schlegel, H.B.: An improved algorithm for reaction path following. J. Chem. Phys. **90**, 2154–2161 (1989)
16. Gonzalez, C., Schlegel, H.B.: Reaction path following in mass-weighted internal coordinates. J. Phys. Chem. **94**, 5523–5527 (1990)
17. Bartlett, R.J.: Many-body perturbation theory and coupled cluster theory for electron correlation in molecules. Annu. Rev. Phys. Chem. **32**, 359–401 (1981)
18. Raghavachari, K., Trucks, G.W., Pople, J.A., Head-Gordon, M.: Quadratic configuration interaction. A general technique for determining electron correlation energies. Chem. Phys Lett. **157**, 479–483 (1989)
19. Olsen, J., Jorgensen, P., Koch, H., Balkova, A., Bartlett, R.J.: Full configuration–interaction and state of the art correlation calculations on water in a valence double-zeta basis with polarization functions. J. Chem. Phys. **104**, 8007–8015 (1996)
20. Dunning Jr., T.H.: Gaussian basis sets for use in correlated molecular calculations. I. The atoms boron through neon and hydrogen. J. Chem. Phys. **90**, 1007–1023 (1989)
21. de Petris, G., Cacace, F., Cipollini, R., Cartoni, A., Rosi, M., Troiani, A.: Experimental detection of theoretically predicted N_2CO. Angew. Chem. **117**, 466–469 (2005)
22. De Petris, G., Rosi, M., Troiani, A.: SSOH and HSSO radicals: An experimental and theoretical study of $[S_2OH]^{0/+/-}$ species. J. Phys. Chem. A **111**, 6526–6533 (2007)
23. Bartolomei, M., et al.: The intermolecular potential in NO-N_2 and $(NO\text{-}N_2)^+$ systems: Implications for the neutralization of ionic molecular aggregates. PCCP **10**, 5993–6001 (2008)
24. Leonori, F., et al.: Observation of organosulfur products (thiovinoxy, thioketene and thioformyl) in crossed-beam experiments and low temperature rate coefficients for the reaction $S(^1D) + C_2H_4$. PCCP **11**, 4701–4706 (2009)
25. Leonori, F., et al.: Crossed-beam and theoretical studies of the $S(^1D) + C_2H_2$ reaction. J. Phys. Chem. A **113**, 4330–4339 (2009)
26. De Petris, G., Cartoni, A., Rosi, M., Barone, V., Puzzarini, C., Troiani, A.: The proton affinity and gas-phase basicity of sulfur dioxide. ChemPhysChem **12**, 112–115 (2011)
27. Berteloite, C., et al.: Low temperature kinetics, crossed beam dynamics and theoretical studies of the reaction $S(^1D) + CH_4$ and low temperature kinetics of $S(^1D) + C_2H_2$. Phys. Chem. Chem. Phys. **13**, 8485–8501 (2011)
28. Rosi, M., Falcinelli, S., Balucani, N., Casavecchia, P., Leonori, F., Skouteris, D.: Theoretical study of reactions relevant for atmospheric models of Titan: Interaction of excited nirogen atoms with small hydrocarbons. LNCS **7333**, 331–344 (2012)
29. Skouteris, D., Balucani, N., Faginas-Lago, N., Falcinelli, S., Rosi, M.: Dimerization of methanimine and its charged species in the atmosphere of Titan and interstellar/cometary ice analogs. Astron. Astrophys. **584**, A76 (2015)
30. Falcinelli, S., Rosi, M., Cavalli, S., Pirani, F., Vecchiocattivi, F.: Stereoselectivity in autoionization reactions of hydrogenated molecules by metastable gas atoms: the role of electronic couplings. Chem. Eur. J. **22**, 12518–12526 (2016)
31. Troiani, A., Rosi, M., Garzoli, S., Salvitti, C., de Petris, G.: Vanadium Hydroxide Cluster Ions in the Gas Phase: Bond-Forming Reactions of Doubly-Charged Negative Ions by SO_2-Promoted V-O Activation. Chem. Eur. J. **23**, 11752–11756 (2017)
32. Rosi, M., et al.: An experimental and theoretical investigation of 1-butanol pyrolysis. Front. Chem. **7**, 326 (2019). https://doi.org/10.3389/fchem.2019.00326

33. Sleiman, C., El Dib, G., Rosi, M., Skouteris, D., Balucani, N., Canosa, A.: Low Temperature Kinetics and Theoretical Study of the Reaction CN + CH3NH2: A Potential Source of Cyanamide and Methyl Cyanamide in the Interstellar Medium. PCCP **20**, 5478–5489 (2018). https://doi.org/10.1039/c7cp05746f
34. Rosi, M., et al.: Possible scenarios for SiS formation in the interstellar medium: electronic structure calculations of the potential energy surdaces for the reactions of the SiH radical with atomic sulphur and S_2. Chem. Phys. Lett. **695**, 87–93 (2018). https://doi.org/10.1016/j.cplett.2018.01.053
35. Balucani, N., Skouteris, D., Ceccarelli, C., Codella, C., Falcinelli, S., Rosi, M.: A theoretical investigation of the reaction between the Amidogen, NH, and the ethyl, C_2H_5, radicals: a possible gas-phase formation route of interstellar and planetary Ethanimine. Molec. Astrophys. **13**, 30–37 (2018). https://doi.org/10.1016/j.molap.2018.10.001
36. Moore, C.E.: Atomic Energy Levels, Natl. Bur. Stand. (U.S.) Circ. N. 467, U.S., GPO, Washington, DC (1949)
37. Gaussian 09, et al. Gaussian, Inc., Wallingford CT (2009)
38. Flükiger, P., Lüthi, H.P., Portmann, S., Weber, J., MOLEKEL 4.3: Swiss Center for Scientific Computing, Manno (Switzerland), (2000–2002)
39. Portmann, S., Lüthi, H. P., MOLEKEL: An Interactive Molecular Graphics Tool Chimia 54, 766–769 (2000)